Prospects for application of ultracold Sr_2 molecules in precision measurements

S. Kotochigova,[1] T. Zelevinsky,[2] and Jun Ye[3]
[1]*Department of Physics, Temple University, Philadelphia, Pennsylvania 19122, USA*
[2]*Department of Physics, Columbia University, 538 West 120th Street, New York, New York 10027-5235, USA*
[3]*JILA, National Institute of Standards and Technology and University of Colorado, Boulder, Colorado 80309-0440, USA*
(Received 9 November 2008; published 8 January 2009)

Precision measurements with ultracold molecules require development of robust and sensitive techniques to produce and interrogate the molecules. With this goal, we theoretically analyze factors that affect frequency measurements between rovibrational levels of the Sr_2 molecule in the electronic ground state. This measurement can be used to constrain the possible time variation of the proton-electron mass ratio. Sr_2 is expected to be a strong candidate for achieving high precision due to the spinless nature and ease of cooling and perturbation-free trapping of Sr [T. Zelevinsky *et al.*, Phys. Rev. Lett. **100**, 043201 (2008)]. The analysis includes calculations of two-photon transition dipole moments between deeply and weakly bound vibrational levels, lifetimes of intermediate excited states, and Stark shifts of the vibrational levels by the optical lattice field, including possibilities of Stark-cancellation trapping.

DOI: 10.1103/PhysRevA.79.012504 PACS number(s): 33.20.−t, 06.20.Jr, 34.80.Qb, 34.50.−s

I. INTRODUCTION

Molecular systems possess a variety of properties that open the possibility to use them for high-precision measurements. The richness of their electronic, vibrational, and rotational spectra provides a series of precision benchmarks from the radio frequencies to the visible spectrum. One of the earliest applications of molecules in spectroscopy involved high accuracy frequency standards. The first molecular clock based on microwave transitions in ammonia was built in 1949 [1]. Other molecular frequency standards provided secondary, relative frequency references to enhance measurement precision [2] and played an important role in measurements of fundamental constants such as the speed of light [3] and possibly the proton-to-electron mass ratio [4].

Furthermore, molecules are valuable for tests of fundamental physics. Diatomic molecules have been proposed for use in parity violation studies [5–7] due to the enhanced sensitivity of rovibrational spectra to nuclear effects, as well as in measurements of the electron electric-dipole moment [8,9], which can benefit from very large internal electric fields of polar molecules.

Recent developments in precision measurement techniques, as well as in cooling and trapping, have stimulated an interest in the application of molecular spectroscopy to studies of possible time variation of fundamental constants [10]. In particular, research has focused on the variation of the fine structure constant α [11] and the proton-to-electron mass ratio $\mu \equiv m_p/m_e$ [12–16]. The values of these constants can drift monotonically, or vary periodically with the distance from the Earth to the Sun in the case of the existence of gravitational coupling. While state-of-the-art optical atomic clocks have set the most stringent limits on both types of α variations [17,18], atoms generally lack transitions that can reveal relative μ variations $(\Delta\mu/\mu)$ in a model-independent way. On the other hand, molecules exhibit complex structure and dynamics due to the combination of their electronic interaction and the vibrations and rotations of their constituent nuclei. For example, if m_p drifts relative to m_e, the effect on the weakly bound vibrational levels near dissociation is expected to be much smaller than on the more deeply bound levels at intermediate nuclear distances [e.g., see Fig. 2(b) in Ref. [12]]. This can allow accurate spectroscopic determinations of $\Delta\mu/\mu$ by using the least sensitive levels as frequency anchors. Moreover, two-color optical Raman spectroscopy of vibrational energy spacings within a single electronic potential takes advantage of the entire molecular potential depth in order to minimize the relative measurement error.

For a given spectral line at frequency ν, the systematic line shift $\Delta\nu$ results from $\Delta\mu$ through the proportionality constant κ:

$$\frac{\Delta\mu}{\mu} = \kappa\frac{\Delta\nu}{\nu}. \tag{1}$$

For direct spectroscopy of molecular vibrational energy levels, $\kappa \sim 1$. To minimize the fractional uncertainty $\delta\mu/\mu$ in the measurement of $(\Delta\mu \pm \delta\mu)/\mu$, we must minimize $\kappa(\delta\nu/\nu)$, where $\delta\nu$ is the measurement uncertainty of the absolute frequency ν. Since in precision spectroscopy experiments the limitations are typically on $\delta\nu$ rather than the relative uncertainty $\delta\nu/\nu$ and since

$$\frac{\delta\mu}{\mu} = \kappa\frac{\delta\nu}{\nu} = \left(\frac{d\nu}{d\ln\mu}\right)^{-1}\delta\nu, \tag{2}$$

the quantity $\nu/\kappa = d\nu/d\ln\mu$ must be maximized. This implies that the optimal frequency intervals for the μ-variation-sensitive molecular clock are those with the largest absolute frequency shifts $(\Delta\nu)$ due to a given fractional change $\Delta\mu/\mu$ (for Sr_2, this is approximately 270 cm^{-1} for a unity change in the mass ratio). In some proposed schemes [10,15], near degeneracies of vibrational levels from different electronic potentials permit a frequency measurement of ν to be carried out in the microwave domain, resulting in a small $\delta\nu$. The effective κ is small, and thus the corresponding quantity ν/κ is reasonably large. In the proposed optical Raman measurement [12], however, the sensitivity enhance-

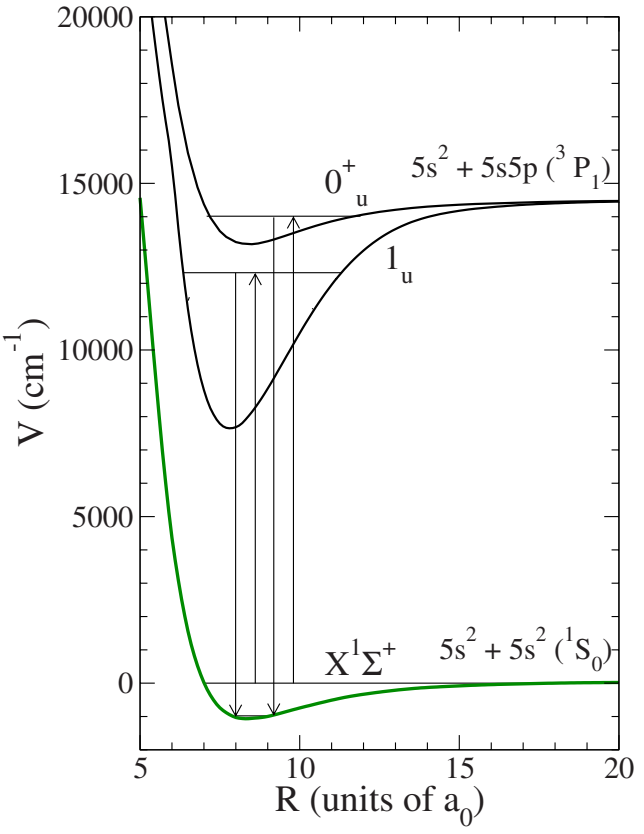

FIG. 1. (Color online) Sr_2 potential energy diagram that shows vibrational levels of the $1(0^+_u)$ and $1(1_u)$ potentials that can be optically excited from vibrational levels of the ground-state potential $X\,^1\Sigma^+$. The energy zero is at the dissociation limit of the ground state.

ment comes from the cumulative shift effect over the depth of the molecular potential. While κ is on the order of unity here, ν is large, resulting in a large ν/κ. Furthermore, if the least sensitive energy gap is measured concurrently with the most sensitive one, it can serve as a reference and thus remove any frequency drift of an intermediate (atomic) clock used in the measurement. Thus, in our previous work [12] we have proposed measuring the intervals between the $Sr_2\ X\,^1\Sigma^+$ (see Fig. 1) vibrational levels $v=27$ (in the middle of the potential well) and $v=-3$ (near dissociation, counting from the top), as well as between $v=27$ and $v=0$. These are complementary schemes, with opposite dependences on $\Delta\mu/\mu$. The difference between these two frequency intervals, normalized by their sum, doubles the sensitivity of the measurement, while eliminating any drift of an intermediate frequency reference used to stabilize the Raman lasers. Finally, all-optical molecular spectroscopy in the tight confinement (Lamb-Dicke) regime in an optical lattice can be Doppler and recoil free, leading to small frequency uncertainties $\delta\nu$.

Ultracold homonuclear molecules in optical lattices are particularly good candidates for high-precision measurements such as those of $\Delta\mu/\mu$. Their vibrational levels have long natural lifetimes that are insensitive to blackbody radiation, and the molecules do not experience long-range interactions when isolated in optical lattice sites. In particular, Sr_2 dimers are promising for precise molecular metrology [12]. Sr atoms can be directly laser cooled to temperatures of $\sim 1\ \mu$K [19,20] and can be trapped in Stark-cancellation optical lattices that eliminate spectral shifts and broadening [21]. Optical atomic clocks based on forbidden electronic transitions in ^{87}Sr have shown that systematic frequency uncertainties can be reduced to the 10^{-16} level [22] in the Lamb-Dicke regime of a Stark-cancellation lattice. Moreover, work on ^{88}Sr narrow-line $^1S_0$-$^3P_1$ photoassociation [23] has shown high experimental efficiency and resolution, and a potential for excellent agreement with theoretical calculations. The comparisons between experiments and theory are largely facilitated by the spinless nature of the ^{88}Sr ground state ($^1S_0$, total electronic angular momentum $J=0$, nuclear spin $I=0$). The electronic ground state of Sr_2 thus corresponds to a single molecular potential ($X\,^1\Sigma^+$ in Fig. 1) with nondegenerate vibrational levels with the exception of rotational duplicity. This simple ground-state potential should allow highly efficient spectroscopic addressing of molecular vibrational levels. Finally, the laser-accessible metastable molecular potentials (corresponding to the $^1S_0+^3P_1$ limit) are expected to have very large Franck-Condon overlaps with the electronic ground state [12,23], further enhancing the atom-molecule conversion efficiency and the Raman molecular vibrational transition strengths.

The proposed mechanism for inducing the vibrational transitions is optical Raman spectroscopy [24], using vibrational levels of metastable Sr_2 as intermediate states. The Sr_2 ground-state electronic potential is 30 THz deep [25], and the Raman lasers can be stabilized to <0.1 Hz relative to each other [26]. Assuming availability of an optical frequency standard [22], a power-broadened linewidth of 10 Hz, and a signal-to-noise ratio of 100, the fractional frequency precision (or, equivalently, the precision of the $\Delta\mu/\mu$ test) approaches $\sim 5\times 10^{-15}/\sqrt{\tau}$, where τ is the averaging time in seconds [12]. Achieving this precision would lead to an important contribution to the μ variation data. Presently, a combination of atomic clock data constrains $\Delta\mu/\mu$ to $\sim 4\times 10^{-16}$/year [17] and the evaluation of astronomical NH_3 spectra constrains $\Delta\mu/\mu$ to $\sim 3\times 10^{-16}$/year [13]. The interpretation of the atomic clock data is dependent on theoretical modeling, since hyperfine transitions depend on both α and μ. The ammonia result is less model dependent, but relies on poorly controllable cosmological observations and disagrees with the cosmological H_2 measurements of $\Delta\mu/\mu$ that indicate nonzero mass ratio variation at the 10^{-15}/year level [27]. An ultracold molecule-based clock for precision measurements would provide a model-independent μ-variation-sensitive system with small, controllable experimental uncertainties.

In this paper we present a detailed analysis of various factors affecting frequency measurements between vibrational levels in the ground state of Sr_2 in an optical lattice. We evaluate transition dipole moments between vibrational levels of the ground and metastable states for determination of the optimal pathways for Raman transitions. In addition, we analyze dynamic polarizabilities of the ground-state vibrational levels in order to identify Stark-cancellation optical lattice frequencies for vibrational transitions. Finally, we estimate the natural linewidths of the intermediate metastable

vibrational levels in order to obtain realistic estimates of spontaneous scattering rates of the optical lattice and Raman spectroscopy photons, and thus of trap losses [12]. The electronic potentials and their properties used in the calculations of the vibrationally averaged dipole moments, polarizabilities, and linewidths are presented in Ref. [28].

II. DIPOLE MOMENTS AND RAMAN TRANSITIONS

For the production of Sr_2 dimers in a particular rovibrational level of the ground-state potential ($X\,^1\Sigma^+$), it is necessary to study the transition dipole moments and transition probabilities between vibrational levels of the $X\,^1\Sigma^+$ and the metastable $1(0_u^+)$ and $1(1_u)$ potentials (dissociating to the $^1S_0+^3P_1$ limit) shown in Fig. 1. The numerical labels (Ω) of the *ungerade* potentials 0_u^+ and 1_u correspond to the total atomic angular momentum projection onto the internuclear axis of 0 and 1, respectively. We choose to work with the metastable intermediate states because of the high spectroscopic resolution and low scattering rates that are possible with narrow lines and due to the large estimated Franck-Condon overlaps with vibrational levels of $X\,^1\Sigma^+$ [12,23]. Preliminary estimates of the transition strengths between weakly bound metastable and ground-state levels were obtained in previous work [23]. However, for precise molecular metrology, more deeply bound vibrational levels must be optically coupled via a Raman scheme. There is no information on these optical transitions in the literature.

The transition dipole moment between vibrational level $v'J'M'$ of an excited-state $\Omega'=0,1$ *ungerade* potential and vibrational level vJM of the ground-state $\Omega=0$ ($X\,^1\Sigma^+$) *gerade* potential is given by

$$\langle \Omega' v' J' M' | d(R) C_{1\epsilon}(\hat{R}) | X\,^1\Sigma^+ v J M \rangle = \langle \Omega' v' J' \| d(R) \| X\,^1\Sigma^+ v J \rangle \times \sqrt{(2J'+1)(2J+1)} \times (-1)^{\epsilon-\Omega'+M} \times \begin{pmatrix} 1 & J & J' \\ -\epsilon & -M & M' \end{pmatrix} \begin{pmatrix} 1 & J & J' \\ -\Omega' & 0 & \Omega' \end{pmatrix}, \tag{3}$$

where $\hat{R}$ is the orientation of the interatomic axis, $C_{1\epsilon}(\hat{R})$ is a spherical harmonic, $\vec{\epsilon}$ is the polarization of the laser field, and M and M' are projections along a laboratory-fixed coordinate axis of the total angular momenta J and J'. The vibrationally averaged or reduced matrix element $\langle \Omega' v' J' \| d(R) \| X\,^1\Sigma^+ v J \rangle$ is a radial integral over the R-dependent relativistic electronic-dipole moment $d(R)$ and rovibrational wave functions of the electronic state $|\Omega'\rangle$ and ground electronic state $|X\,^1\Sigma^+\rangle$.

We study transitions to both metastable potentials dissociating to $^1S_0+^3P_1$ (Fig. 1). Figures 2 and 3 show the squares of the vibrationally averaged dipole moments as a function of vibrational energies of the potentials $1(0_u^+)$ and $1(1_u)$, respectively, in atomic units $(ea_0)^2$, where e is the electron charge and $a_0=0.053$ nm is the Bohr radius. A comparison of the two figures shows that the squares of the dipole moments for $1(0_u^+)$ are two orders of magnitude larger than for $1(1_u)$ for deeply bound levels. This is due to the difference in strengths of the electronic transition dipole moments at small separations (shown in Fig. 4) and the similarity in shape of the $X\,^1\Sigma^+$ and $1(0_u^+)$ potentials. This similarity also explains the localized character of Franck-Condon factors for a given vibrational level of the $X\,^1\Sigma^+$ state (see Fig. 2). However, for weakly bound levels with binding energies less than 500 cm^{-1} the squared dipole moments for the two potentials have similar magnitudes. The electronic-dipole moments near the outer turning points have similar magnitudes, and the $1(0_u^+)$ and $1(1_u)$ potentials are more similar in shape. In our analysis of Raman transition rates we will focus on the $1(0_u^+)$ potential since it has favorable dipole moments with the ground state.

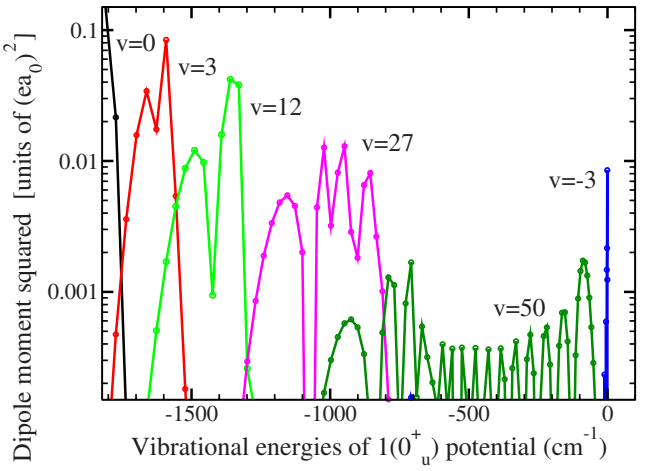

FIG. 2. (Color online) The square of the vibrationally averaged dipole moments for transitions from selected vibrational levels (all with $J=0$) of the $X\,^1\Sigma^+$ electronic ground state as a function of the energy of vibrational levels (with $J'=1$) of the $1(0_u^+)$ potential of Sr_2. Each curve corresponds to a single rovibrational level of the X state. Zero energy corresponds to the $^1S_0+^3P_1$ dissociation limit.

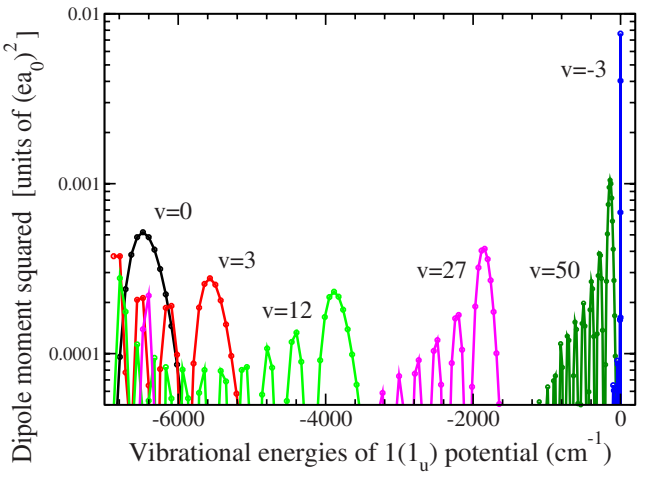

FIG. 3. (Color online) The square of the vibrationally averaged dipole moments for transitions from selected vibrational levels (all with $J=0$) of the $X\,^1\Sigma^+$ electronic ground state as a function of the energy of vibrational levels (with $J'=1$) of the $1(1_u)$ potential of Sr_2. Each curve corresponds to a single rovibrational level of the X state. Zero energy corresponds to the $^1S_0+^3P_1$ dissociation limit.

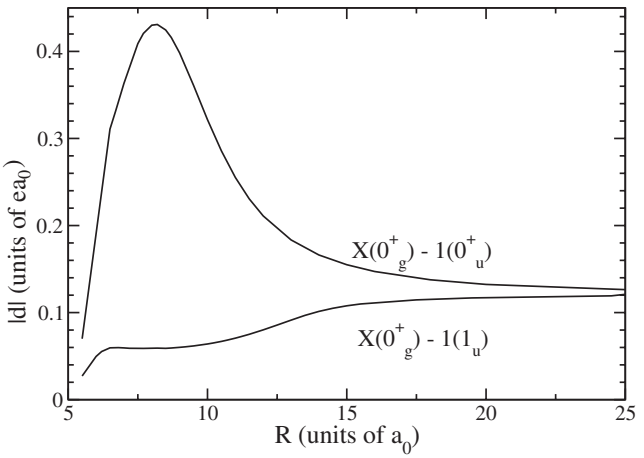

FIG. 4. Absolute values of electronic transition dipole moments from the $X\,^1\Sigma^+$ ground state to the metastable states $1(0_u^+, 1_u)$ of Sr_2. Adapted from [28].

A Raman transition is the process by which we transfer population from an initially occupied vibrational level to a final level via an intermediate state. In this case, both the initial and final levels are $J=0$ rovibrational levels of the $X\,^1\Sigma^+$ potential, while the intermediate level is a $J'=1$ rovibrational level of $1(0_u^+)$. The Rabi matrix element for this two-photon process is proportional to the product of the dipole moments of both transitions. We chose the weakly bound $v=-3$ level of the $X\,^1\Sigma^+$ potential as the initial Raman state, since it is expected to be most efficiently populated by photoassociation [23]. Figure 5 shows the dipole moment products for the $v=-3$ initial state and the $v=27$ final state as a function of the vibrational energy of the $1(0_u^+)$ potential. This pathway was selected in Ref. [12] for the precision measurement of possible variations of the proton to electron mass ratio.

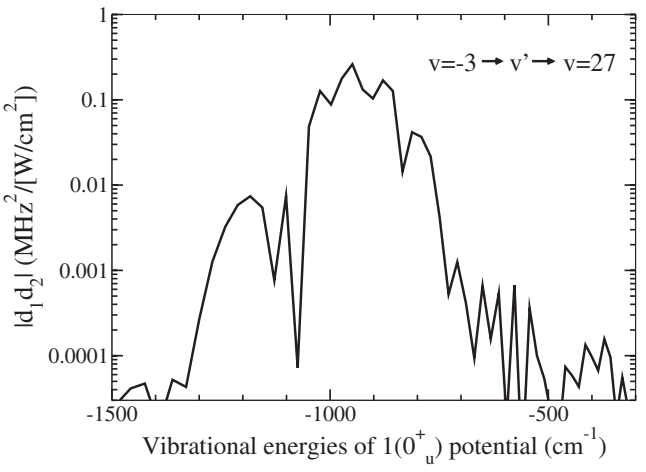

FIG. 5. Two-photon vibrationally averaged dipole moments for the Raman transitions as a function of the energies of v', $J'=1$ rovibrational levels of the $1(0_u^+)$ intermediate state. The pathway that was proposed in Ref. [12] is shown. It starts from the $v=-3$, $J=0$ rovibrational level and ends at the $v=27$, $J=0$ level of the $X\,^1\Sigma^+$ ground state. The energy zero corresponds to the $^1S_0+^3P_1$ dissociation limit.

III. STARK SHIFTS IN AN OPTICAL LATTICE

Trapping ultracold molecules in optical lattices via ac Stark shifts is key for optimized control and precision [12]. Optical lattice traps benefit both the reduction of systematic effects and the achievement of high molecule densities on the order of $10^{12}/\mathrm{cm}^3$ [23]. The Stark-cancellation, or *magic frequency*, technique [21] has enabled state-of-the-art neutral atom clocks [18]. This approach relies on a suitable crossing of dynamic polarizabilities of the two probed states at a particular lattice wavelength. This ensures a zero differential Stark shift and a suppression of the inhomogeneous Stark broadening. Analogously, Stark-cancellation optical lattice frequencies can be sought for specific pairs of the Sr_2 vibrational levels. For example, tuning the lattice frequency near a narrow resonance associated with an optical transition from a vibrational level of $X\,^1\Sigma^+$ to another one of $1(1_u)$ can help achieve matching polarizabilities of a vibrational level pair of $X\,^1\Sigma^+$.

The ac Stark shifts of the vibrational levels of illuminated ground-state molecules are determined by the dynamic polarizability $\alpha(h\nu, \vec{\epsilon})$, which is a function of the radiation frequency ν and polarization $\vec{\epsilon}$ (h is the Planck constant). If the Sr_2 molecule is in the ground-state potential $X\,^1\Sigma^+$, its dynamic polarizability in SI units is expressed in terms of the dipole coupling to the rovibrational levels of the excited potentials as

$$\alpha(h\nu,\vec{\epsilon}) = \frac{1}{\epsilon_0 c}\sum_f \frac{(E_f - ih\gamma_f/2 - E_i)}{(E_f - ih\gamma_f/2 - E_i)^2 - (h\nu)^2} \times |\langle f|d(R)\hat{R}\cdot\vec{\epsilon}|i\rangle|^2, \quad (4)$$

where c is the speed of light, ϵ_0 is the electric constant, $\langle f|d|i\rangle$ are R-dependent electric-dipole moments (containing both radial and angular contributions), and i and f denote the initial $|vJM\rangle$ and intermediate $|v'J'M'\rangle$ rovibrational wave functions of the $X\,^1\Sigma^+$ and Ω' electronic states, respectively. The energy E_i is the rovibrational energy of the $X\,^1\Sigma^+$ state, and E_f is the rovibrational energy of the Ω' state. Finally, the linewidths γ_f describe the spontaneous and other decay and loss mechanisms. Equation (4) is a sum over dipole transitions to the rovibrational levels of excited potentials; this includes contributions from the continuum of the Ω' states as well. This sum can be truncated if transitions have negligible electric-dipole moments or large detunings. In the case of Sr_2, the sum only includes contributions from potentials with $\Omega'=0,1$ and *ungerade* symmetry. The potentials and transition dipole moments are calculated in Ref. [28].

The frequency of the optical lattice is in the near-infrared range, where the laser can be tuned close to a transition from a ground-state vibrational level to a vibrational level of the $1(1_u)$ potential (Fig. 1). We employ two approaches to finding either vibrational levels with the same Stark shift or the Stark-cancellation light frequency for a given pair of levels. The first approach is to analyze the dependence of the baseline molecular polarizability on the vibrational quantum number for a fixed laser frequency and look for nonmonotonic behavior, thus allowing certain pairs of vibrational levels to have the same Stark shifts. The second approach is to

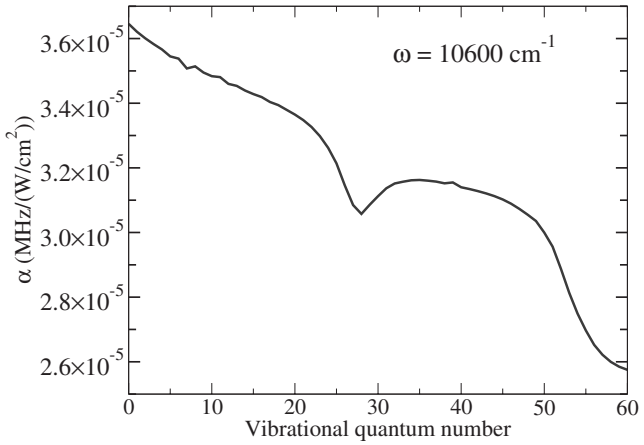

FIG. 6. Real part of the dynamic polarizability α of the $J=0$ levels of the $X\,^1\Sigma^+$ ground state of Sr_2 as a function of vibrational quantum number for infrared laser frequency of 10 600 cm^{-1}.

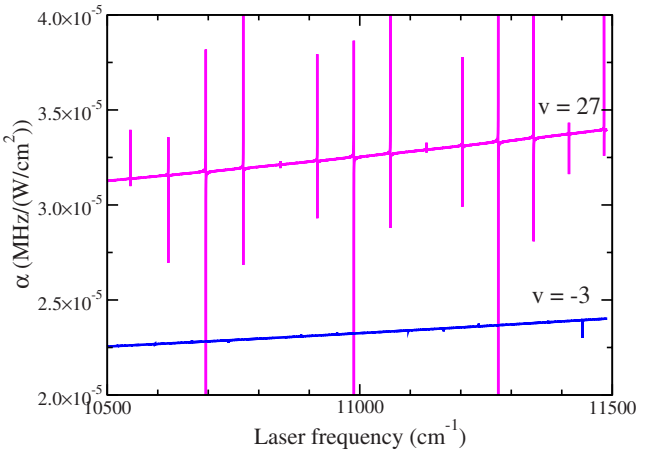

FIG. 7. (Color online) Real part of the dynamic polarizability of the $J=0$ vibrational levels of the Sr_2 $X\,^1\Sigma_g^+$ state as a function of laser frequency in the range of 10 500–11 500 cm^{-1}. For clarity, only two selected vibrational levels of the X state are shown, $v=-3$ and $v=27$. The polarizabilities are evaluated at 0.1-cm^{-1} intervals. The polarizabilities of $J=0$ rotational levels are independent of the laser polarization.

rely on sharp polarizability resonances arising from presence of vibrational levels in the metastable potentials as shown in Fig. 1. While the latter method allows significantly more flexibility, care must be taken to ensure low incoherent photon scattering rates [12].

For simultaneous trapping of Sr_2 molecules in different vibrational levels of the $X\,^1\Sigma^+$ potential in a Stark-cancellation regime, we can use the first approach and search for vibrational levels of $X\,^1\Sigma^+$ that have equal polarizabilities. Figure 6 shows the dynamic polarizability at the infrared laser frequency of 10 600 cm^{-1} as a function of the vibrational quantum number of the $X\,^1\Sigma^+$ potential for the rotational level $J=0$. The polarizability tends to decrease with increasing vibrational quantum number; exceptions occur for $v>27$ vibrational levels. Analysis of the individual contributions to the polarizability shows that the dip near $v=27$ is due to an avoided crossing between relativistic $\Omega=1$ excited potentials, which coincides with the outer turning point of the $v=27$ vibrational level of the ground-state potential. As a result, we can find matching polarizabilities for the higher vibrational levels. However, there is a possibility that this dip is an artifact of our method of calculation. We assumed that the vibrational motion is purely adiabatic, which might not be accurate for this avoided crossing. It would require a multichannel calculation of the vibrational levels to test our results.

The second approach to matching the polarizabilities of different vibrational levels makes use of resonances. The calculated molecular polarizabilities of the Sr_2 ground-state vibrational levels of interest are shown in Fig. 7 as a function of laser frequency in the vicinity of 910 nm, which is near the Stark-cancellation wavelength for the $^1S_0$-$^3P_1$ transition for atomic ^{88}Sr. The overall polarizabilities are determined by the base-line value of $\alpha \sim (2-4)\times 10^{-5}$ MHz/(W/cm^2) arising from far-detuned dipole-allowed transitions to states dissociating to the $^1S_0$-$^1P_1$ atomic limit, as well as by the resonant structure due to narrow vibrational levels of the $1(1_u)$ potential dissociating to the $^1S_0$-$^3P_1$ limit. Figure 7 shows three resonances in the range of 10 700–11 300 cm^{-1} with matching polarizabilities for the $v=-3$ and $v=27$ vibrational levels.

The profiles of these resonances are determined by Franck-Condon factors between the vibrational levels of the $X\,^1\Sigma^+$ and $1(1_u)$ potentials. The natural linewidths of the $1(1_u)$ levels are below 10^{-6} cm^{-1}, which is negligible on the frequency scale of Fig. 7. A blowup of one of the resonances in Fig. 7 near the frequency of 10 988 cm^{-1} is shown in our previous publication [12]. An optical lattice frequency near this resonance was identified for Stark cancellation of the two ground-state vibrational levels.

Other resonances could be chosen for optical lattice frequencies to facilitate precision measurements—for example, those in the laser frequency range of 13 500–14 600 cm^{-1}. These resonances arise from transitions between vibrational levels of the $X\,^1\Sigma^+$ and $1(0_u^+)$ potentials. Figure 8 shows many such resonances with matching polarizabilities for the $v=-3$ and $v=27$ vibrational levels. Choosing to work near these resonances requires caution regarding the possibly enhanced scattering of the lattice light. Previously, we have estimated the incoherent scattering rates of only $\sim 1/s$ with 10 kW/cm^2 laser intensities [12], using the calculated spontaneous decay rates of $1(1_u)$ (Sec. IV) and the transition dipole moments (Sec. II).

The exact locations of the resonances shown in Figs. 7 and 8 must be refined with the additional input of experimental data. To date, fewer than ten most weakly bound states of $1(0_u^+)$ and $1(1_u)$ have been experimentally identified [23]. However, the general polarizability trends, the density of vibrational levels, and the relative line strengths are expected to remain close to our present predictions.

IV. NATURAL LINEWIDTHS OF EXCITED VIBRATIONAL LEVELS

Linewidths of the vibrational levels of the $1(0_u^+)$ and $1(1_u)$ potentials are important for estimating incoherent scattering

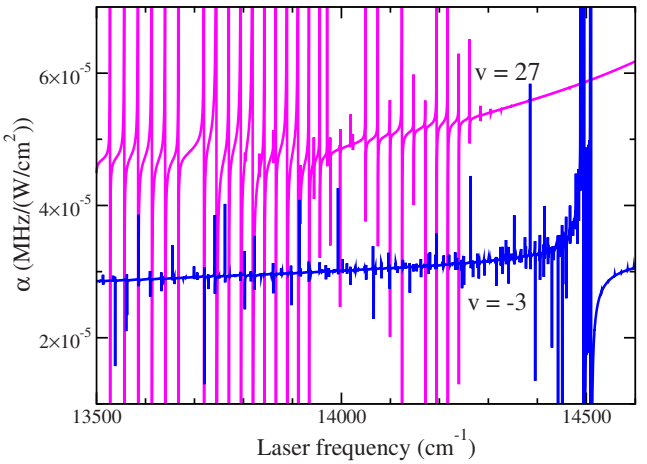

FIG. 8. (Color online) Real part of the dynamic polarizability of the $J=0$ vibrational levels of the Sr_2 $X\,^1\Sigma_g^+$ state as a function of laser frequency in the range of 13 500–14 600 cm^{-1}. For clarity, only two selected vibrational levels of the X state are shown, $v=-3$ and $v=27$. The polarizabilities are evaluated at 0.1-cm^{-1} intervals. The polarizabilities of $J=0$ rotational levels are independent of the laser polarization.

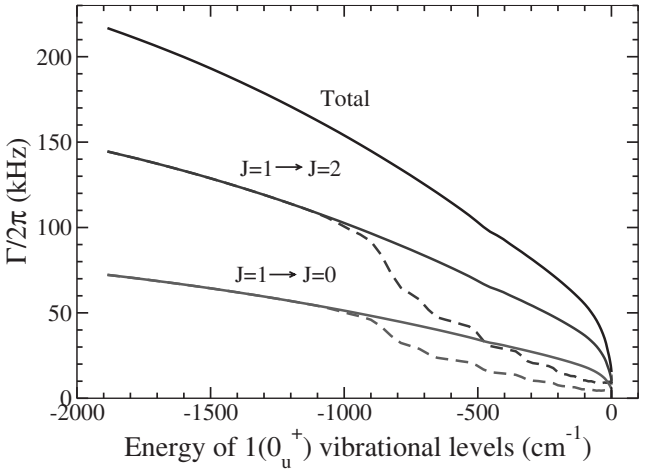

FIG. 9. Natural linewidths of the $1(0_u^+)$ vibrational levels of Sr_2 as a function of their energy. The individual contributions from the $(J=1\rightarrow J=0)$ and $(J=1\rightarrow J=2)$ pathways are shown. Dashed lines indicate contributions from bound-bound transitions. The zero energy corresponds to the $^1S_0+^3P_1$ dissociation limit.

rates of the Raman spectroscopy light and of the Stark-cancellation optical lattice trap, as well as of near-resonant Stark shifts [12]. The natural decay rate of the vibrational level $v'J'M'$ of an excited potential Ω' is given by the Einstein A coefficient in s^{-1},

$$A=\frac{8\pi}{3hc^3}\sum_{\epsilon,vJM}\omega_{vJ}^3\times|\langle\Omega' v'J'M'|d(R)C_{1\epsilon}(\hat{R})|X\,^1\Sigma^+ vJM\rangle|^2, \tag{5}$$

where the sum is over all light polarizations ϵ and quantum numbers vJM of the ground-state potential, v can denote either vibrational states or continuum scattering states, and the quantities $\omega_{vJ}/(2\pi)$ are the transition frequencies from the excited vibrational level to the ground-state rovibrational level $|vJ\rangle$.

Figures 9 and 10 show natural linewidths of the vibrational levels of the excited $1(0_u^+)$ and $1(1_u)$ potentials for all binding energies. The linewidths contain contributions from transitions between $J=1$ rotational levels of the $1(0_u^+)$ and $1(1_u)$ potentials to $J=0$ and $J=2$ rotational levels of the ground state. These are the only relevant rotational levels, since only $J=1$ metastable levels are populated with photoassociation of the spinless ^{88}Sr atoms. The values and trends of the linewidths are primarily determined by the R-dependent dipole moments between the metastable and ground states plotted in Fig. 4. For most weakly bound levels, the linewidths approach 15 kHz, in good agreement with twice the linewidth of the $^3P_1$ atomic limit [23]. For deeply bound levels with outer turning points below $14a_0$, the transition dipole moments and linewidths are significantly larger for the $1(0_u^+)$ potential than for $1(1_u)$.

Figures 9 and 10 also show the contributions of bound-bound transitions to the linewidths. For the deepest and the most weakly bound vibrational levels, nearly all natural decay is into the bound states. This is explained by the similar shapes of the ground state and metastable potentials at small and large internuclear separations. Previous work [23] indicated single-vibrational-channel decay efficiencies up to 90% for weakly bound states. The equilibrium internuclear separations are very similar for the ground state and both metastable states, which explains the high bound-bound decay efficiencies for the deeply bound molecules. At intermediate binding energies, the continuum of the ground state contributes significantly to the linewidths.

V. CONCLUSION

We have investigated the properties of Sr_2 that are relevant to the development of precision measurement tech-

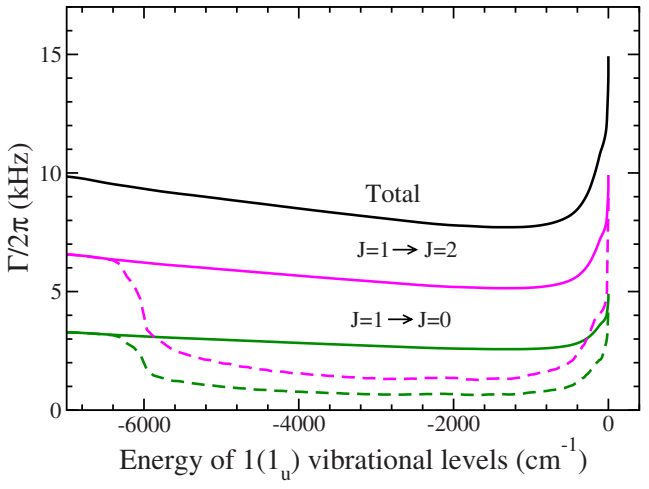

FIG. 10. (Color online) Natural linewidths of the $1(1_u)$ vibrational levels of Sr_2 as a function of their energy. The individual contributions from the $(J=1\rightarrow J=0)$ and $(J=1\rightarrow J=2)$ pathways are shown. Dashed lines indicate contributions from bound-bound transitions. The zero energy corresponds to the $^1S_0+^3P_1$ dissociation limit.

niques with ultracold molecules. The experimental and theoretical input from our previous work [23,28] has allowed us to carry out realistic calculations of the two-photon Raman transition strengths between two targeted vibrational levels in the ground state via an intermediate metastable state. We find the results to favor single-step transfer from the weakly bound to intermediate vibrational levels of Sr_2 in the ground state. Further, we have explored two approaches to implementing Stark-cancellation optical lattice traps for Sr_2. We find that the method relying on polarizability resonances should allow Stark-shift-free trapping with low molecule losses. The relatively small photon scattering rates are determined by the optical transition strengths as well as by the total decay rates of the vibrational levels in the metastable electronic state, which are calculated including the bound-bound and bound-continuum contributions. The combination of ultracold temperatures, perturbation-free trapping, efficient optical transfer, and low environmental sensitivity of Sr_2 should allow effective production and precise manipulation and measurements with this molecule.

ACKNOWLEDGMENTS

We acknowledge financial support from AFOSR, ARO, NIST, and NSF.

[1] C. H. Townes, J. Appl. Phys. **22**, 1365 (1951).
[2] J. Ye, L. S. Ma, and J. L. Hall, Phys. Rev. Lett. **87**, 270801 (2001).
[3] K. M. Evenson, J. S. Wells, F. R. Petersen, B. L. Danielson, G. W. Day, R. L. Barger, and J. L. Hall, Phys. Rev. Lett. **29**, 1346 (1972).
[4] J. C. J. Koelemeij, B. Roth, A. Wicht, I. Ernsting, and S. Schiller, Phys. Rev. Lett. **98**, 173002 (2007).
[5] M. G. Kozlov and L. N. Labzovsky, J. Phys. B **28**, 1933 (1995).
[6] V. V. Flambaum and J. S. M. Ginges, Phys. Rev. A **74**, 025601 (2006).
[7] D. DeMille, S. B. Cahn, D. Murphree, D. A. Rahmlow, and M. G. Kozlov, Phys. Rev. Lett. **100**, 023003 (2008).
[8] M. G. Kozlov and D. DeMille, Phys. Rev. Lett. **89**, 133001 (2002).
[9] J. J. Hudson, B. E. Sauer, M. R. Tarbutt, and E. A. Hinds, Phys. Rev. Lett. **89**, 023003 (2002).
[10] V. V. Flambaum and M. G. Kozlov, Phys. Rev. Lett. **99**, 150801 (2007).
[11] E. R. Hudson, H. J. Lewandowski, B. C. Sawyer, and J. Ye, Phys. Rev. Lett. **96**, 143004 (2006).
[12] T. Zelevinsky, S. Kotochigova, and J. Ye, Phys. Rev. Lett. **100**, 043201 (2008).
[13] V. V. Flambaum and M. G. Kozlov, Phys. Rev. Lett. **98**, 240801 (2007).
[14] A. Shelkovnikov, R. J. Butcher, C. Chardonnet, and A. Amy-Klein, Phys. Rev. Lett. **100**, 150801 (2008).
[15] D. DeMille, S. Sainis, J. Sage, T. Bergeman, S. Kotochigova, and E. Tiesinga, Phys. Rev. Lett. **100**, 043202 (2008).
[16] V. V. Flambaum and M. G. Kozlov, e-print arXiv:0711.4536.
[17] T. Rosenband, D. B. Hume, P. O. Schmidt, C. W. Chou, A. Brusch, L. Lorini, W. H. Oskay, R. E. Drullinger, T. M. Fortier, J. E. Stalnaker, S. A. Diddams, W. C. Swann, N. R. Newbury, W. M. Itano, D. J. Wineland, and J. C. Bergquist, Science **319**, 1808 (2008).
[18] S. Blatt, A. D. Ludlow, G. K. Campbell, J. W. Thomsen, T. Zelevinsky, M. M. Boyd, J. Ye, X. Baillard, M. Fouché, R. Le Targat, A. Brusch, P. Lemonde, M. Takamoto, F.-L. Hong, H. Katori, and V. V. Flambaum, Phys. Rev. Lett. **100**, 140801 (2008).
[19] H. Katori, T. Ido, Y. Isoya, and M. Kuwata-Gonokami, Phys. Rev. Lett. **82**, 1116 (1999).
[20] T. H. Loftus, T. Ido, M. M. Boyd, A. D. Ludlow, and J. Ye, Phys. Rev. A **70**, 063413 (2004).
[21] J. Ye, H. J. Kimble, and H. Katori, Science **320**, 1734 (2008).
[22] A. D. Ludlow, T. Zelevinsky, G. K. Campbell, S. Blatt, M. M. Boyd, M. H. G. de Miranda, M. J. Martin, J. W. Thomsen, S. M. Foreman, Jun Ye, T. M. Fortier, J. E. Stalnaker, S. A. Diddams, Y. Le Coq, Z. Barber, N. Poli, N. D. Lemke, K. M. Beck, and C. W. Oates, Science **319**, 1805 (2008).
[23] T. Zelevinsky, M. M. Boyd, A. D. Ludlow, T. Ido, J. Ye, R. Ciurylo, P. Naidon, and P. S. Julienne, Phys. Rev. Lett. **96**, 203201 (2006).
[24] K.-K. Ni, S. Ospelkaus, M. H. G. de Miranda, A. Pe'er, B. Neyenhuis, J. J. Zirbel, S. Kotochigova, P. S. Julienne, D. S. Jin, and J. Ye, Science **322**, 231 (2008).
[25] E. Czuchaj, M. Krośnicki, and H. Stoll, Chem. Phys. Lett. **371**, 401 (2003).
[26] A. D. Ludlow, X. Huang, M. Notcutt, T. Zanon-Willette, S. M. Foreman, M. M. Boyd, S. Blatt, and J. Ye, Opt. Lett. **32**, 641 (2007).
[27] E. Reinhold, R. Buning, U. Hollenstein, A. Ivanchik, P. Petitjean, and W. Ubachs, Phys. Rev. Lett. **96**, 151101 (2006).
[28] S. Kotochigova, J. Chem. Phys. **128**, 024303 (2008).